*Kufa Journal of Engineering*
*Vol. 17, No. 1, January 2026, P.P. 157-175*
*Article history: Received 8 October 2024, last revised 29 December 2024, accepted 25 January 2025*

# INVESTIGATION OF FLUID FLOW BEHAVIOR IN FIXED AND ADJUSTABLE HYDRAULIC CHANNELS

**Ahmed Zamzeer[1], Zainab Al-Khafaji[2,3], Talib Abdulameer Jasim[4], Mohammad Qraywi[2], Mayadah Falah[5], and Sabaa Radhi[1]**

**[1] Mechanical Engineering, Altinbas University, İstanbul, Turkey.**

**[2] Department of Civil Engineering, Faculty of Engineering and Built Environment, Universiti Kebangsaan Malaysia, Bangi, Selangor, Malaysia, Email:P123005@siswa.ukm.edu.my.**

**[3] New Era and Development in Civil Engineering Research Group, Scientific Research Center, Al-Ayen University, Thi-Qar, 64001, Iraq.**

**[4] Department of Aeronautical Technical Engineering, College of Technical Engineering, Al-Farahidi University, Baghdad, Iraq, Email:talib-abd@uoalfarahidi.edu.iq.**

**[5] Building and Construction Techniques Engineering Department, College of Engineering and Engineering Techniques, AL-Mustaqbal University, 51001, Babylon, Iraq.**

**https://doi.org/10.30572/2018/KJE/170109**

## ABSTRACT

Challenges of open-channel flow are discussed, with emphasis on energy dissipation and the difficulties brought by channel design for hydraulic pressure and velocity measure. The influence of the rheology of the slurry on channel design is also complicated. The objective of this work is to study the flow behavior in open channels of different shapes and with variable wall stability (fixed and movable). ANSYS Fluent (Release 2, 2021) Computational Fluit Dynamic (CFD) simulations were performed for the velocity distribution and pressure profiles in four configurations of channels: parallel, zigzag, wavy and curved. The study examines the effects of channel height variations and various inlet velocity (6, 3, and 0.3 m/s) on flow behavior. Findings indicate that increasing channel height reduces internal pressure, while lowering the height increases it, with pressure also varying by channel geometry. The curved channel shows the maximum pressure at a height of 0.5 m, and the channel with wavy shape exhibits the maximum pressure at 2831.92 MPa, with the curved channel reaching 3384.85 MPa under fixed-wall conditions.

**KEYWORDS**

Channels shapes, Fixed and movable channels, Computational Fluid Dynamics (CFD).

## 1. INTRODUCTION

A deep hollow surface with its top surface often subject to the surroundings is called an open channel (Al-Bedyry et al., 2023). Open channel flow is the movement of a fluid across a deep hollow surface (channel) that has an atmosphere-covered top surface (Al-Naely, Al-Khafaji, et al., 2019; Al-Naely, Majdi, et al., 2019; Tao et al., 2024). Rivers, lakes, ditches, sewers, flumes, and streams are examples of open channels in motion (Khlewee et al., 2024; Tao et al., 2021). A passage for flow of fluid under air pressure is called an open channel (Al-Khafaji et al., 2022). Conversely, a fluid that is flowing under pressure—involving that which flows through sewage pipes—is referred to as being in closed-channel flow or pressurized flow, where the flow is entirely enclosed within the conduit, and its behavior is governed by pressure variances rather than open atmospheric interaction (Roshankhah et al., 2023). Open-channel flow is often classified based on its uniformity. The flow is deemed steady if the velocity at any observation location does not change over time; if it does, the flow is deemed unsteady. The flow was shown to be uniform when the velocity was always constant throughout the channel; the flow has been demonstrated to be non-uniform. Variable flow is non-uniform flow that is unstable, while varying flow is non-uniform flow that is also stable. The movement of substances from a region of higher concentration to a lower concentration is a fundamental process influenced by various factors, including gravity (Benedini & Tsakiris, 2013; Wu, 2015). This phenomenon, commonly referred to as diffusion, is central to the understanding of many natural and engineered systems. Diffusion entails the passive transport of particles down their concentration gradient, driven by molecular motion and other physical forces.

Numerical investigations on different channel geometries have been conducted. Tokgoz, (2019) employed Particle Image Velocimetry (PIV) to obtain detailed information during an investigation of the flow patterns within corrugated ducts. In this context, the PIV technique was applied in their experiment to gain essential insights regarding the flow phenomena inside corrugated channels. The features of flow are investigated as four characteristic function Reynolds numbers, i.e., Re = 2000-5000. Based on the findings, it is possible that corrugation of the channel enhanced energy and momentum transmission, which resulted in an increase in heat transfer rate. The entrainment between the wake and core flows above was mainly owing to the onset of turbulence in a corrugated channel near a sharp-corner geometry. The experimental findings were confirmed by calculations, using the identical model geometry and position of measurements obtained in the side view plane. Data comparison presented that the pattern of velocity profile changed continually and there was a well compatibility between experimental and simulation findings. A curved wavy channel has been proposed by (Zhang et

al., 2022) to improve the existing wavy channel thermal performance. With the development of a 3D model of the curved wavy channel, the overall curvature was determined. Interaction analysis between the temperature fields and velocity revealed the mechanism underlying the observed behaviors. The findings show that the Nusselt numbers in curved wavy channels may be increased by 15.3 and 44.3percent, respectively, in contrast to the traditional wavy channels with amplitudes of 0.80 mm and 0.40 mm. In determining the heating transfer intensity in the channel with relatively small wavelengths, the field synergy angle has limitations. This occurs because very chaotic flow patterns caused by narrow wavelengths generate negative partial derivatives of temp variance and velocity over a large region.

According to (Memon et al., 2021) used Galerkin's approach's least square technique to analyze the steady flow of a Newtonian fluid down a sine-curved channel. Using Comsol Multiphysics 5.4, the entire simulation is practiced. Sine-curved channels were used with amplitudes between 10 cm and 30 cm and Reynolds numbers between 1000 and 10,000 to investigate the fluid flow through these channels. The pressure and flow rates were checked at the exit. The maximum pressure settled into a negative relationship with the Reynolds number as the Reynolds number grew, and the maximum speed is recorded to grow linearly along the Reynolds number at the exit. A comprehensive three-dimensional, two-phase CFD model for flow distribution in an open channel was examined by (Khazaee & Mohammadiun, 2012). The finite volume method (FVM) with a dynamic Sub grid-scale has been utilized in seven cases with varying proportions, inclination degrees or slopes, and convergence divergence circumstances. Utilizing the volume of fluid (VOF) technique, the free surface was let to change freely in line with the underlying turbulence. The velocity-area integration method is frequently used to calculate the discharge through open channel flow from the measured velocity at discrete sites in the measuring section. Thus, it is crucial to consider the fluctuation of velocity in both horizontal and vertical directions when choosing where to place the sensors. (Harikrishnan et al., 2021) used finite volume-based open-source field operations and modification to numerically examine flow transition mechanisms in wavy channels. Kelvin-Helmholtz and centrifugal instabilities are shown by the two wavy channel forms. Sinusoidal walls with out-phase and in-of-phase channel topologies were considered. By changing Reynolds number, two channel topologies change steady flow to chaotic. Detailed flow regime maps are given for the two wavy channel layouts. iso-Q surfaces, vorticity contours, velocity contours, and Instantaneous streamlines showed unstable flow features. Cross correlation recurrence quantification study revealed coordinated channel flow. SOP setup with Re=200 and 220 organizes vortices approximately symmetrically around the centerline. The first two dominating unstable modes have an alternate vortex pattern in the

flow direction. SIP setup with Re = 102 showed a spanwise vortex pattern. Re increased vortex' flow direction inclination

Open-channel flow poses several special difficulties; energy loss, hydraulic pressure and velocity profiles depend on the rheological behaviour of the fluid as well as the form of channel. While flow behaviour has been studied in various channels, there is a lack of detailed interaction between flow stability with velocity and pressure at different geometry for multiple inlet configurations at different conditions. Experimental investigations, such as those by (Bahaidarah, 2009), indicated augmented flow characteristics in wavy channels, but did not fully consider the intricate relationship between geometry and flow stability. Numerical experiments of (Harikrishnan & Tiwari, 2020; Khazaee & Mohammadiun, 2012) investigated instabilities associated with wavy channels, but the effect of channel geometry on pressure and velocity has not been addressed systematically for various types of flow. The present study fills these gaps by a characterization of flow over four different open-channel configurations (namely, parallel, zigzag, wavy, and curved) through Computational Fluid Dynamics (CFD). To explore how the aspect ratio of channel geometry affects velocity and pressure distributions, in this work our focus on providing a better understanding about nature characteristic of flow stability tendency and pressure change behaviour under different geometries. In addition, this article investigates the effect of variation in channel height and inlet velocity (6, 3 and 0.3 m/s) on flow behavior. The significance of this work is to provide a comprehensive understanding of the geometric and stability relationship in diverse types of open-channels, resulting in improved design parameters for near-optimal open-channel systems uses (i) hydraulic engineering applications, and (ii) flow management facilities.

## 2. THREE-DIMENSIONAL MESH GENERATION

Dividing this process into subsequent steps, with two major meshing control difficulties, would make it more robust.

### 2.1. Meshing the Models

(Stebbins et al., 2019) described the domains, channel boundary types, exit and entrance area kinds (velocity outlet and inlet), and geometry built with a single volume. Consequently, the channels' walls were generated by employing a similar meshing technique with quad dominant, and the construction has been meshed using T-grid tetrahedral components technique. The ANSYS grid generator, which consists of around 3 to 4.5 million computational cells, was

selected for multiple scenarios. As explained in Fig. 1, the grids for the wavy channel are configured.

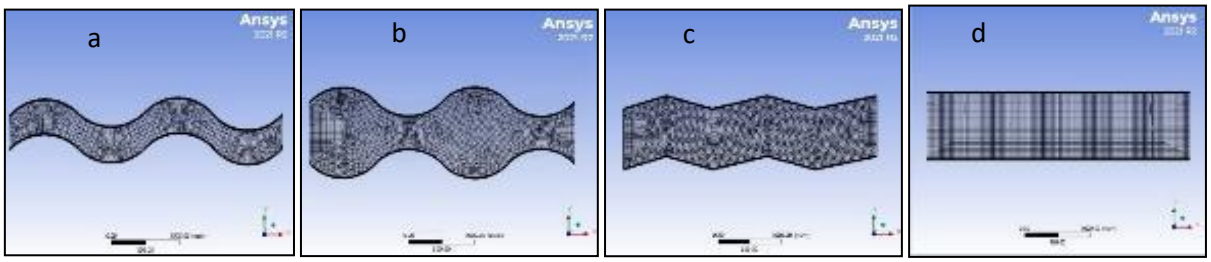


**Fig. 1. Channel computational grids: (a) parallel; (b) wavy; (c) zigzag; (d) curvature.**

## 2.2. Governing Equations

Most CFD difficulties seem to be based on the solutions to the (mass, energy, and momentum) equations and the transportation equation for simulating turbulence viscosity and the scaling. These were clearly stated below and appeared to be in a stable state (ANSYS, 2011).

Regarding chaotic flow:

**Mass Conservation**

$$\frac{\partial \bar{u}}{\partial x}+\frac{\partial \bar{v}}{\partial y}+\frac{\partial \bar{w}}{\partial z}=0 \tag{1}$$

Momentum Conservation (Navier-Stokes formula)

$$\left(\bar{u}\frac{\partial \bar{u}}{\partial x}+\bar{v}\frac{\partial \bar{u}}{\partial y}+\bar{w}\frac{\partial \bar{u}}{\partial z}\right)+\left(\frac{\partial}{\partial x}\left(\overline{u'^2}\right)+\frac{\partial}{\partial y}\left(\overline{u'v'}\right)+\frac{\partial}{\partial z}\left(\overline{u'w'}\right)\right)=-\frac{1}{\rho}\frac{\partial p}{\partial x}+\frac{\mu}{\rho}\left(\frac{\partial^2 \bar{u}}{\partial x^2}+\frac{\partial^2 \bar{u}}{\partial y^2}+\frac{\partial^2 \bar{u}}{\partial z^2}\right) \tag{2}$$

$$\left(\bar{u}\frac{\partial \bar{v}}{\partial x}+\bar{v}\frac{\partial \bar{v}}{\partial y}+\bar{w}\frac{\partial \bar{v}}{\partial z}\right)+\left(\frac{\partial}{\partial x}\left(\overline{u'v'}\right)+\frac{\partial}{\partial y}\left(\overline{v'^2}\right)+\frac{\partial}{\partial z}\left(\overline{u'w'}\right)\right)=-\frac{1}{\rho}\frac{\partial p}{\partial y}+\frac{\mu}{\rho}\left(\frac{\partial^2 \bar{v}}{\partial x^2}+\frac{\partial^2 \bar{v}}{\partial y^2}+\frac{\partial^2 \bar{v}}{\partial z^2}\right) \tag{3}$$

$$\left(\bar{u}\frac{\partial \bar{w}}{\partial x}+\bar{v}\frac{\partial \bar{w}}{\partial y}+\bar{w}\frac{\partial \bar{w}}{\partial z}\right)+\left(\frac{\partial}{\partial x}\left(\overline{u'w'}\right)+\frac{\partial}{\partial y}\left(\overline{u'v'}\right)+\frac{\partial}{\partial z}\left(\overline{w'^2}\right)\right)=-\frac{1}{\rho}\frac{\partial p}{\partial z}+\frac{\mu}{\rho}\left(\frac{\partial^2 \bar{w}}{\partial x^2}+\frac{\partial^2 \bar{w}}{\partial y^2}+\frac{\partial^2 \bar{w}}{\partial z^2}\right) \tag{4}$$

Energy Conservation

$$\left(\bar{u}\frac{\partial \bar{T}}{\partial x}+\bar{v}\frac{\partial \bar{T}}{\partial y}+\bar{w}\frac{\partial \bar{T}}{\partial z}\right)+\left(\frac{\partial}{\partial x}\left(\overline{u'T'}\right)+\frac{\partial}{\partial y}\left(\overline{v'T'}\right)+\frac{\partial}{\partial z}\left(\overline{w'T'}\right)\right)=\alpha\left(\frac{\partial^2 \bar{T}}{\partial x^2}+\frac{\partial^2 \bar{T}}{\partial y^2}+\frac{\partial^2 \bar{T}}{\partial z^2}\right) \tag{5}$$

Turbulence Kinetic Energy formula

$$\rho\left(\bar{u}\frac{\partial k}{\partial x}+\bar{v}\frac{\partial k}{\partial y}+\bar{w}\frac{\partial k}{\partial z}\right)=\left[\left(\mu+\frac{\mu_t}{\sigma_k}\right)\left(\frac{\partial^2 k}{\partial x^2}+\frac{\partial^2 k}{\partial y^2}+\frac{\partial^2 k}{\partial z^2}\right)\right]+G_k-\rho\epsilon \tag{6}$$

Boussines hypothesis

$$G_k=\mu_t\times S^2 \tag{7}$$

$$S\equiv\sqrt{2S_{ij}S_{ij}} \tag{8}$$

$$S_{ij}=\frac{1}{2}\left(\frac{\partial \bar{u_\iota}}{\partial x_j}+\frac{\partial \bar{u_j}}{\partial x_i}\right) \tag{9}$$

whereas:

*Sij*: The strain tensor's average rate of change.

The eddy viscosity in turbulent flows

$$\mu_t = \rho C_\mu \frac{k^2}{\epsilon} \quad (10)$$

The magnitudes of the modeling constants have been identified using RNG theory. These settings are used by ANSYS Fluent by default.

### 2.3. The Boundary Conditions

The proper specification of boundary conditions is essential for accurate CFD simulations, particularly when solving the Navier-Stokes, mass, and energy equations. In the present investigation, boundary conditions were specified carefully to guarantee validation of the FLUENT calculations. Table 1 Boundary conditions for outlet and inlet of the computational domain imposed. The flow parameters at the boundaries of the physical model 5 (involving velocity, pressure and temperature) are characterized by means of boundary conditions. At the base of the channel a no-slip condition was employed, respecting to the main design characteristic of this channel. This guarantees that the fluid velocity normal to the boundary is zero, an essential assumption of practical applications. Physical dimensions and flow behavior within fixed and movable setups of the channel were well represented in selected boundary conditions. By these approximations and boundary definitions, the number of variables dramatically decreased that gave a computationally simplifying analysis as well as more reliable findings.

### 2.4. Checking For Convergence

Monitoring the residuals (Zakhour et al., 2023) is an approach to testing the convergence of the solution. Convergence occurs when all the parameters' requirements for convergence are satisfied. If the residuals mentioned above (10–4) and (10–7) are satisfied, the solution is deemed to be converging. As seen in Fig. 2, all the scaling residuals were significantly lower than 10-4 and 10-7. Using a computer cluster with 8 nodes, each with an Intel® CORE(TM) i7 CPU running at 1.65 GHz and 8 GB of RAM, it normally takes more than 300 iterations to get a converged result, which usually takes around 30 minutes.

### 2.5. Turbulence Intensity

In the two phases, the intensity of turbulence (I) is expressed as the ratio of fluctuations in velocity ($\acute{u}$) to the mean velocity ($u_{ave}$). The magnitude of turbulence at the center of a completely constructed channel flow may be determined using the following equations, which were derived from an equation for flow fluid.

$$I = \frac{\acute{u}}{u_{ave}} = 0.16 \times (Re)^{-1/8} \quad (11)$$

The typical intensity of the turbulence set was five percent (medium intensity) (ANSYS, 2011).

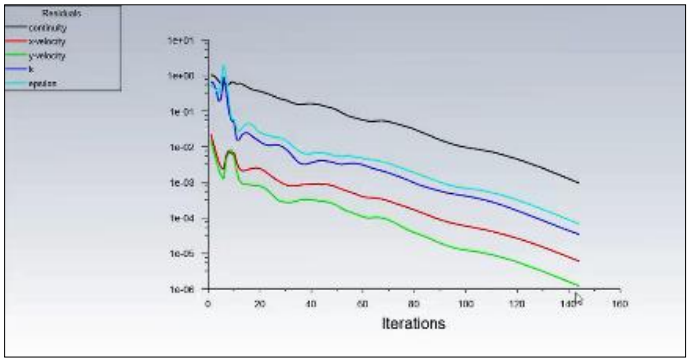


**Fig. 2. Convergence history of solving discrete conservation equations.**

**Table 1. Various channels details obtained from ANSYS software program.**

| Objects | Parallel | Zigzag | Wavy | Curved |
|---|---|---|---|---|
| **Sizing** | | | | |
| Bounding Box Diagonal (mm) | 4123.1 | 4179 | 4087.6 | 4257.6 |
| Mean Surface Area ($mm^2$) | $4x10^6$ | $4 x10^6$ | $2.0408 x10^6$ | $4.0036 x10^6$ |
| Min Edge Length (mm) | 1000 | 704.47 | 500 | 1000 |
| **Statistic** | | | | |
| Nodes | $0.5628x10^4$ | $0.6027x10^4$ | $0.3980x10^4$ | $0.6253x10^4$ |
| Elements | $0.5453x10^4$ | $0.5853x10^4$ | $0.3816x10^4$ | $0.6073x10^4$ |

## 2.6. Simulation Cases

The scenarios for modeling fluid in various channel geometries, utilized to investigate the impact of channel geometries on fluid dynamics, are detailed in Table 2.

**Table 2. Outline for all chosen cases situations.**

| Sets ID | Details | | |
|---|---|---|---|
| | Case 1 (velocity=0.3 m/s) | Case 2 (velocity=3 m/s) | Case 3 (velocity=6 m/s) |
| | **Fixed channels with viscous fluid and different heights (m)** | | |
| 1 | 0.5 | 0.5 | 0.5 |
| 2 | 1 | 1 | 1 |
| 3 | 1.5 | 1.5 | 1.5 |
| | **Moving channels with viscous fluid and different heights (m)** | | |
| 4 | 1 | 1 | 1 |

# 3. RESULTS AND DISCUSSION

This section delineates the numerical findings acquired for numerous factors, including channel morphology, movement, wall stability, and flow type, pertaining to parallel, wavy, zigzag, and curved channels. The influence of different channel layouts is further shown with graphs showing changes in velocity and pressure.

## 3.1. Impact of Velocity Variation on 0.5m Height

Fig.3-6 illustrated the variations in velocity inside the channel for several configurations (parallel, wavy, curved, and zigzag) when the velocity inlet was altered to 6, 3, and 0.3 m/s, with a channel height of 0.5 m. Fig.3-6 depicts the disparity in velocity between the velocity intake and the mean velocity for an open channel including several wall configurations (parallel, wavy, curved, and zigzag). The findings indicate that the curvature channel exhibits the greatest

mean velocity of 13.78 m/s among all examined instances, whilst the zigzag channel is the lowest average velocity relative to the other channel configurations. Furthermore, the findings indicated that the channel's geometry influences the velocity within the channel by modifying the adjacent layer, which subsequently leads to changes in pressure and the formation of vortices, thereby creating a velocity disparity.

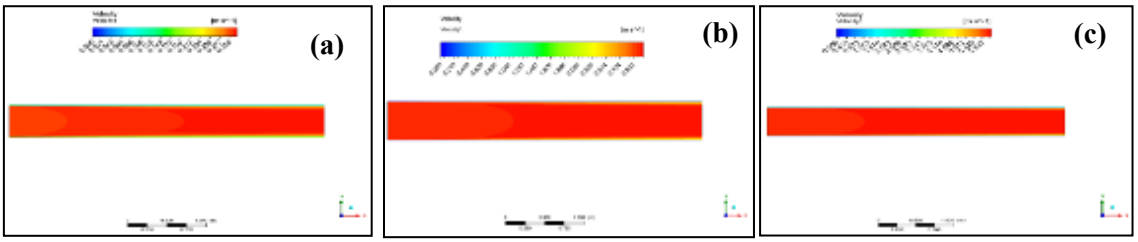


**Fig. 3. Velocity for parallel channels geometry for set 1 case: (a) 1; (b) 2; (c) 3.**

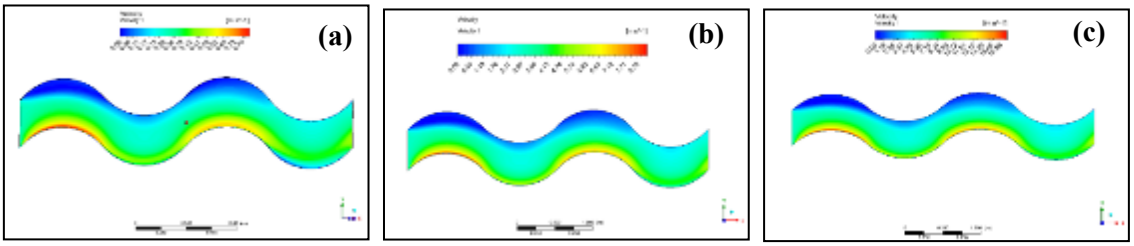


**Fig. 4. Velocity for wavy channels geometry for set 1 case: (a) 1; (b) 2; (c) 3.**

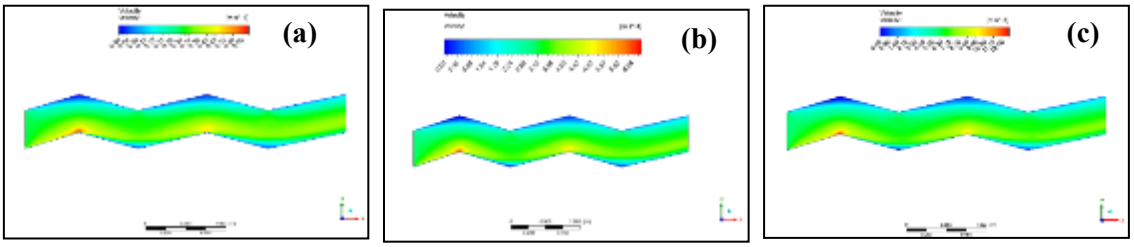


**Fig. 5. Velocity for zigzag channels geometry for set 1 case: (a) 1; (b) 2; (c) 3.**

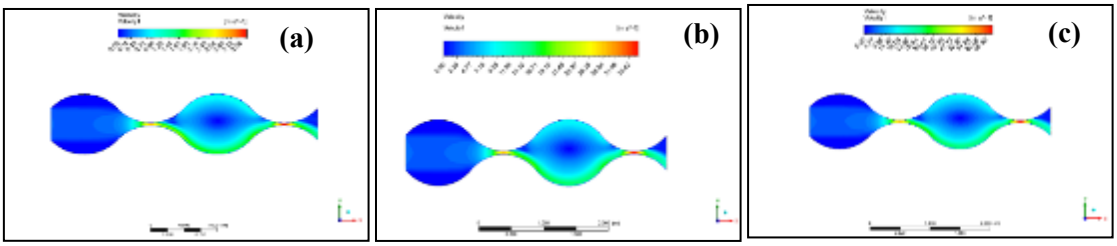


**Fig. 6. Velocity for curvature channels geometry for set 1 case: (a) 1; (b) 2; (c) 3.**

Figs.7 to 11 showed the variance of entry pressure and velocity in different channel structures. The findings indicate that when along the curved channel, the pressure and velocity variance are largest. The variance in findings between curved and parallel is remarkable. The argument is that different geometries of the neighboring layers create a larger number of vortices. The large gap in the geometry of the next layer creates great variances between curved and straight. This variance is caused by the increased production of vortices (Tran et al., 2017).

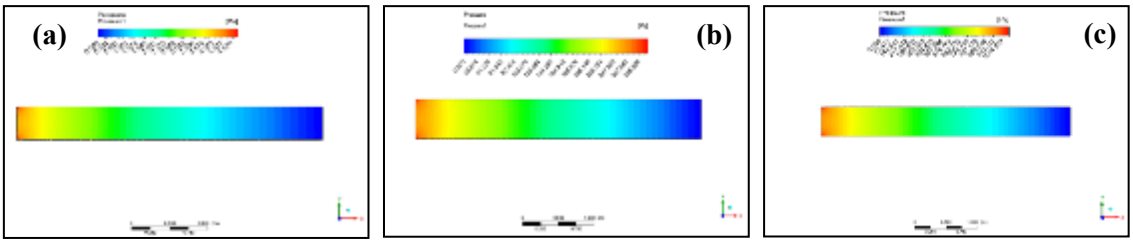


**Fig. 7. Pressure for parallel channels geometry for set 1 case: (a) 1; (b) 2; (c) 3.**

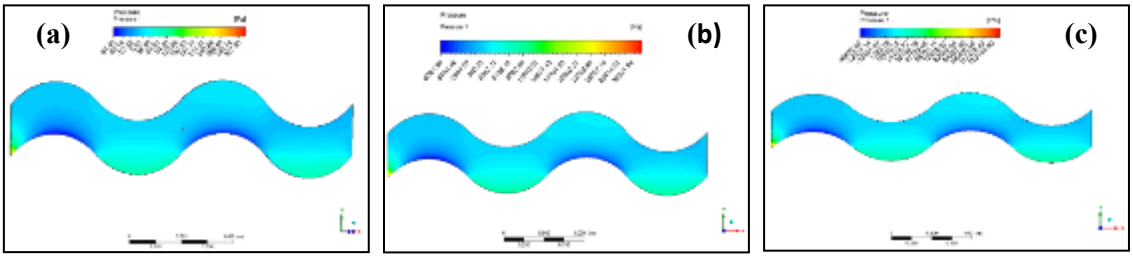


**Fig. 8. Pressure for wavy channels geometry for set 1 case: (a) 1; (b) 2; (c) 3.**

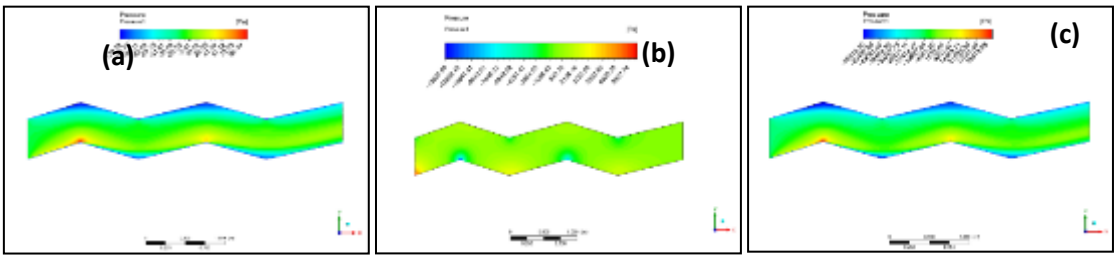


**Fig. 9. Pressure for zigzag channels geometry for set 1 case: (a) 1; (b) 2; (c) 3.**

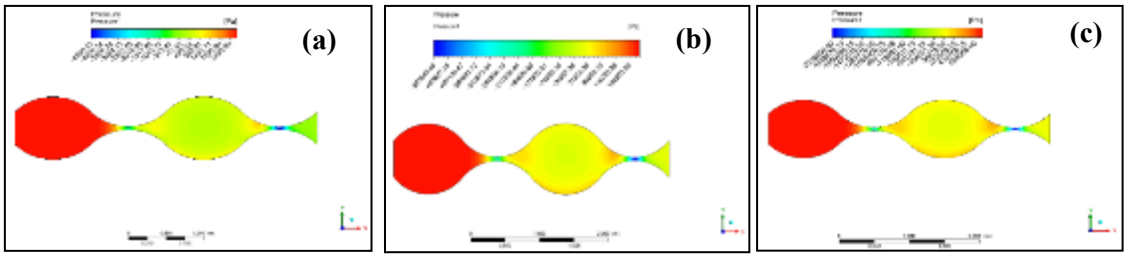


**Fig. 101. Pressure for curvature channels geometry for set 1 case: (a) 1; (b) 2; (c) 3.**

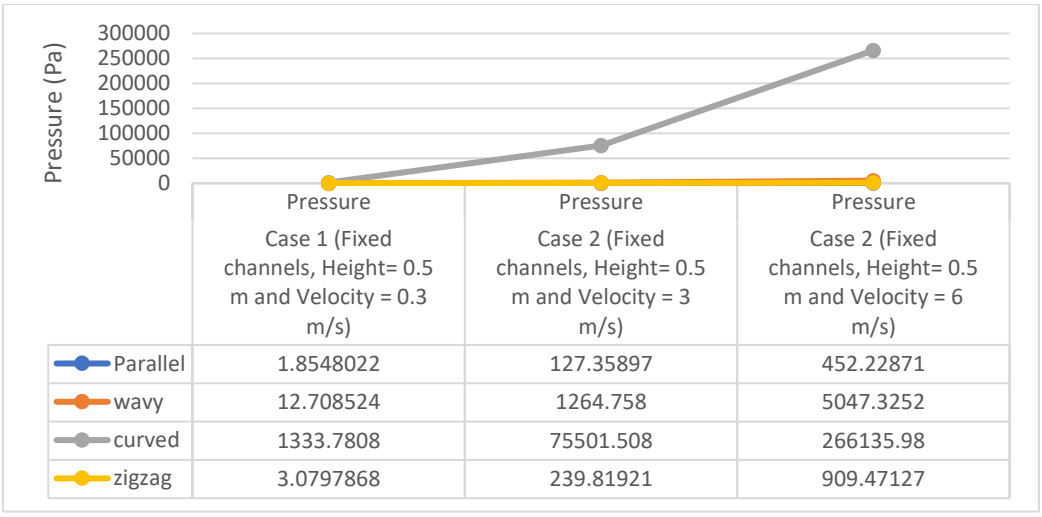


| | Pressure Case 1 (Fixed channels, Height= 0.5 m and Velocity = 0.3 m/s) | Pressure Case 2 (Fixed channels, Height= 0.5 m and Velocity = 3 m/s) | Pressure Case 2 (Fixed channels, Height= 0.5 m and Velocity = 6 m/s) |
|---|---|---|---|
| Parallel | 1.8548022 | 127.35897 | 452.22871 |
| wavy | 12.708524 | 1264.758 | 5047.3252 |
| curved | 1333.7808 | 75501.508 | 266135.98 |
| zigzag | 3.0797868 | 239.81921 | 909.47127 |

**Fig. 11. The impact of velocity variations (6, 3, and 0.3 m/s) on pressure for different channel geometries in set 1.**

### 3.2. Impact of Velocity Variation on 1m Height

Figs. 12 to 15 illustrate the variations in velocity across several channel geometries (parallel, wavy, zigzag, and curved) under three distinct scenarios with entrance velocities of 6, 3, and 0.3 m/s, revealing a consistently low velocity dispersion despite the alterations in entry velocity magnitudes. The wavy channel had the maximum velocity among all examined input velocities, measuring 6.19 m/s.

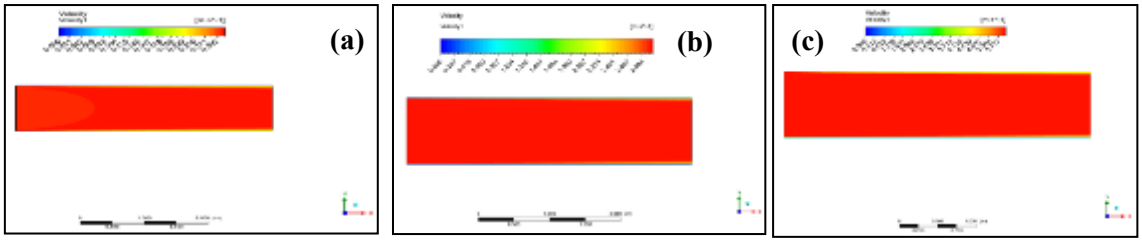


**Fig. 12. Velocity for parallel channels geometry for set 2, viscous fluid and velocity (m/s): (a) 0.3; (b) 3; and (c) 6.**

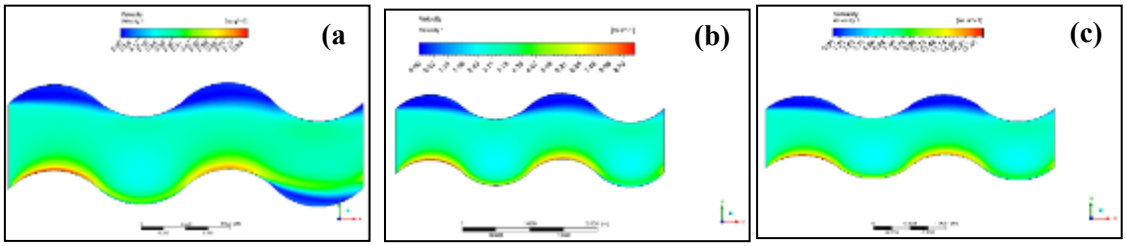


**Fig. 13. Velocity for wavy channels geometry for set 2 cases: (a) 1; (b) 2; (c) 3.**

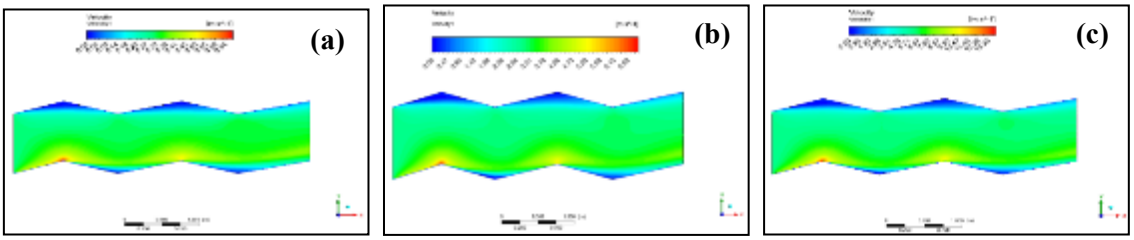


**Fig. 14. Velocity for zigzag channels geometry with for set 2 cases: (a) 1; (b) 2; (c) 3.**

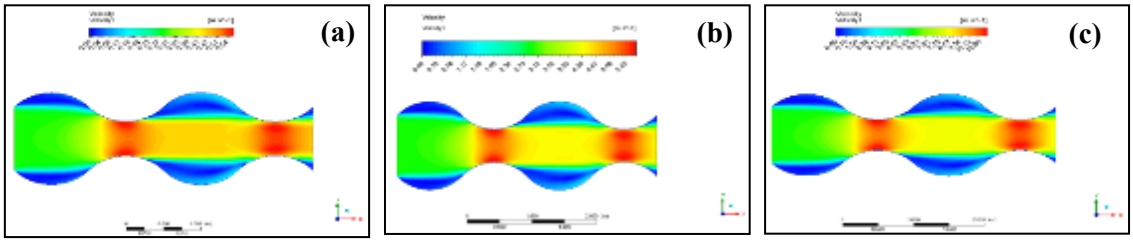


**Fig. 15. Velocity for curvature channels geometry for set 2 cases: (a) 1; (b) 2; (c) 3.**

Figs. 16-19 show selected profiles of the ratio of input velocity and pressure for different channel geometries. The pressure and maximum velocity are both normalized as zero for the curved channel configuration with a height of '1 meter' in this case study with fixed channel's wall. The large variance in the findings between the curved and parallel channels is because the different channel geometry, even if they have similar input height and velocity. To induce the flow regime shift from laminar to turbulent, which can be represented by a larger vortex and a

considerable pressure variance (Nezu & Nakagawa, 2017). In addition, the pressure in this study grew as the input velocity increased for all selected channel types where the maximum pressure value was found in wavy channel with approximately 2831.92 MPa in comparison to other type of channels.

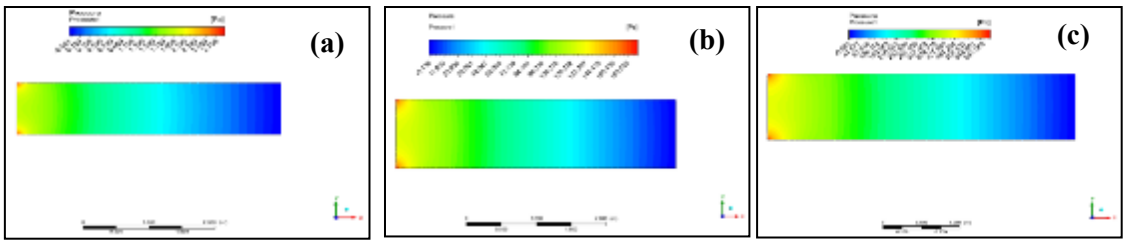


**Fig. 16. Pressure for parallel channels geometry for set 2 cases: (a) 1; (b) 2; (c) 3.**

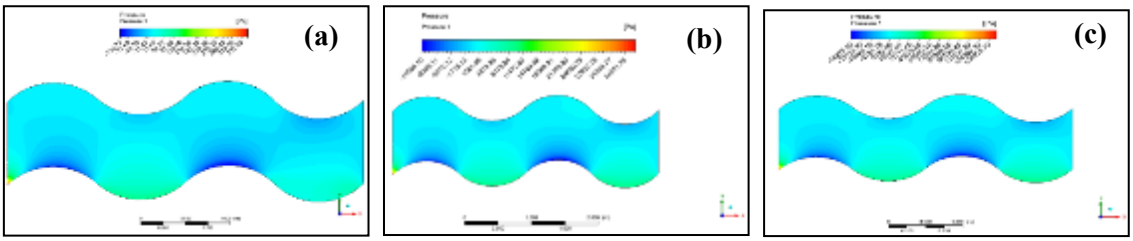


**Fig. 17. Pressure for wavy channels geometry for set 2 cases: (a) 1; (b) 2; (c) 3.**

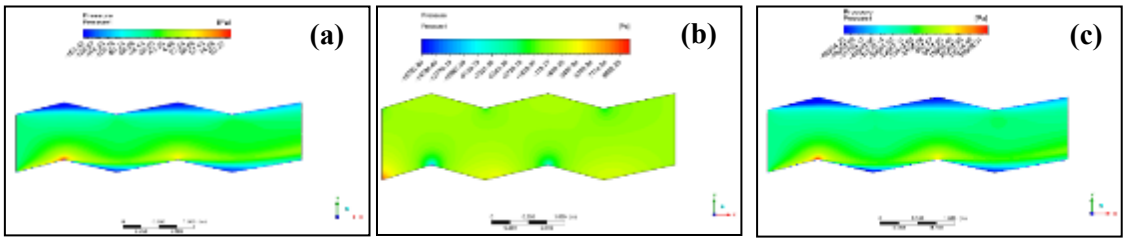


**Fig. 18. Pressure for zigzag channels geometry for set 2 cases: (a) 1; (b) 2; (c) 3.**

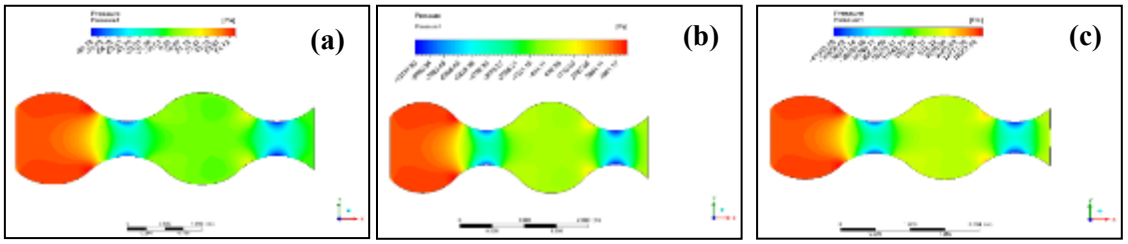


**Fig. 19. Pressure for curvature channels geometry for set 2 cases: (a) 1; (b) 2; (c) 3.**

### 3.3. Impact of Velocity Variation on 1.5m Height

Figs.20 to 23 demonstrate the influence of variation in velocity entry from (6, 3, and 0.3 m/s) for channel height equivalent to 1.5 m on the velocity inside the channel in various channel forms (wavy, curved, parallel, and zigzag). The distribution of velocity for different channel geometries with a height of 1.5 meters is comparable to that of channels with a height of 1 meter but with lower velocities. This discovery accords with Bernoulli's Principle, which suggests an adverse correlation between height and velocity (Kumari & Kumar, 2022).

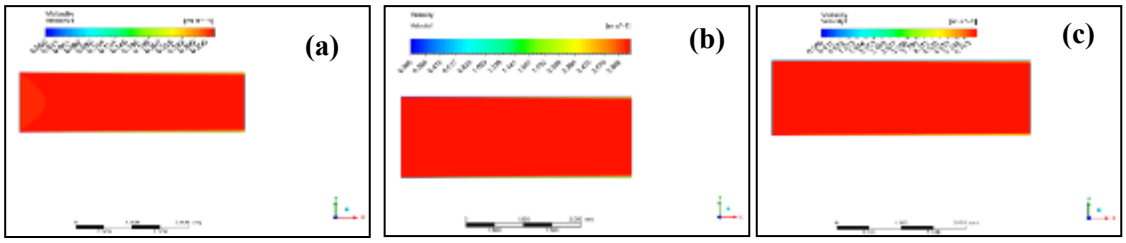


**Fig. 20. Velocity for parallel channels geometry for set 3 cases: (a) 1; (b) 2; (c) 3.**

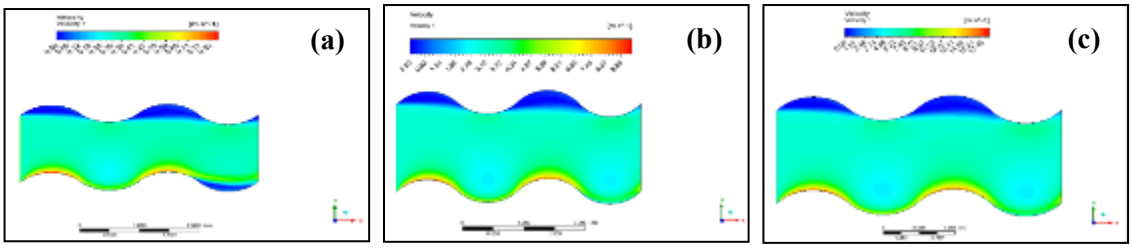


**Fig. 21. Velocity for wavy channels geometry for set 3 cases: (a) 1; (b) 2; (c) 3.**

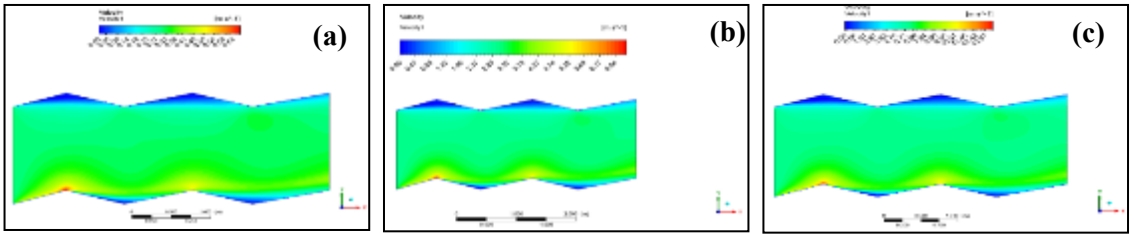


**Fig. 22. Velocity for zigzag channels geometry for set 3 cases: (a) 1; (b) 2; (c) 3.**

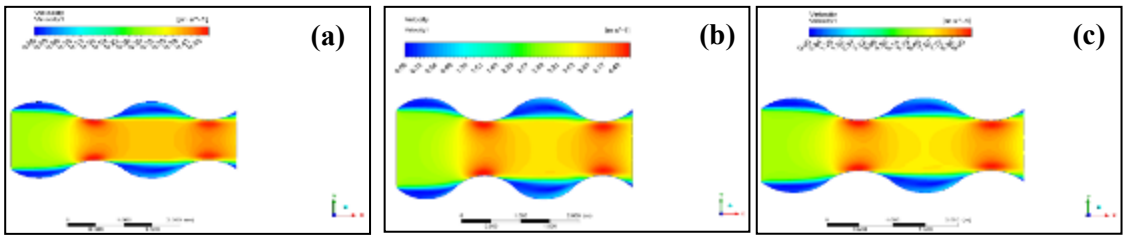


**Fig. 23. Velocity for curvature channels geometry for set 3 cases: (a) 1; (b) 2; (c) 3.**

The modification in the channel's elevation findings in changes in both pressure and velocity. The present set illustrates the pressure fluctuations following the increase in the amplitude of channels with diverse geometrical forms (parallel, wavy, zigzag, and curved) to 1.5m, as depicted in Figs.24 to 27, respectively. Figs. 24 to 27 illustrates that the curvature channels register reverse pressure magnitude for all designated entry velocities, with an increase in velocity from 0.3 to 6 m/s leading to a transition from positive to negative pressure magnitudes of (-1009.22 MPa). The objective is to reduce the channel's width in some sections while expanding it in places designated for the curved channel. The reduction in channel width leads to in increased velocity for equivalent discharges once the relationship between velocity and cross-sectional area is inversely proportional; an increase in one findings in to a reduction in the other, as dictated by the Continuity Equation (Seis, 2017). Conversely, the relationship between cross-sectional area and pressure is directly proportional, according to Bernoulli's principle (Kumari & Kumar, 2022).

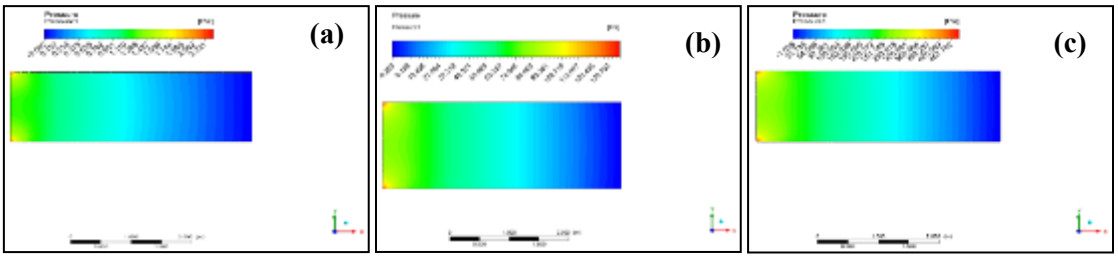


**Fig. 24. Pressure for parallel channels geometry for set 3 cases: (a) 1; (b) 2; (c) 3.**

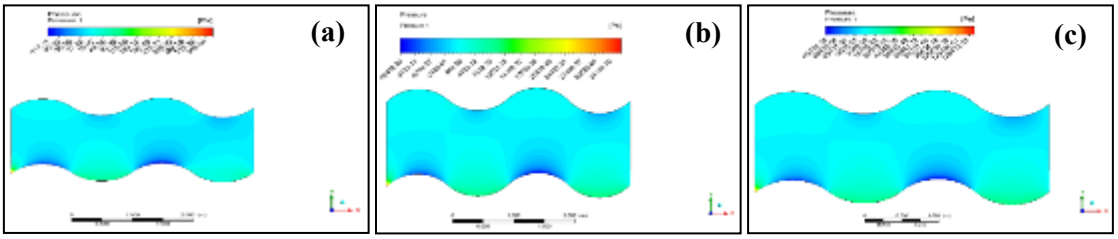


**Fig. 25. Pressure for wavy channels geometry for set 3 cases: ( a) 1; (b) 2; (c) 3.**

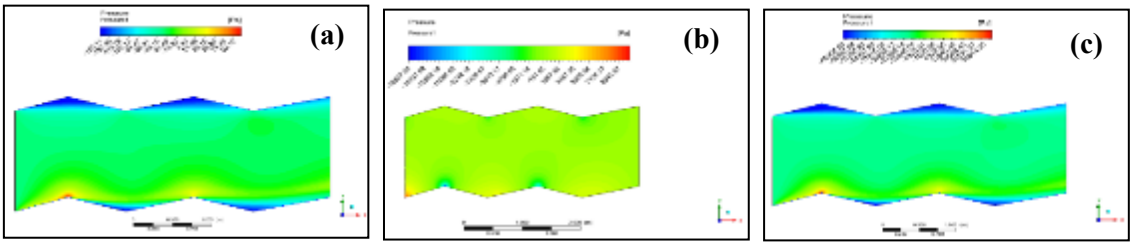


**Fig. 262. Pressure for zigzag channels geometry for set 3 cases: (a) 1; (b) 2; (c) 3.**

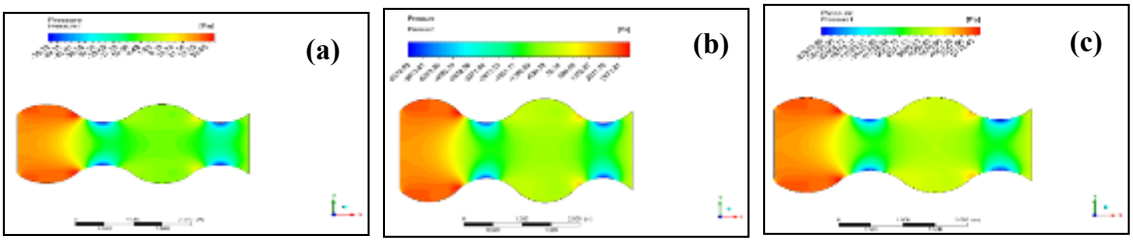


**Fig. 27. Pressure for curvature channels geometry for set 3 cases: (a) 1; (b) 2; (c) 3.**

### 3.4. Impact of Walls Stability and Movement

The variances between the entry velocity and velocity variance for different channels with anchored and shifting walls are displayed in Figs.28 to 31, for set four with shifting wall of channels, the height = 1m, viscous fluid and velocity a) 0.3 m/s b) 3 m/s, and c) 6 m/s., when comparing this set with the second set, the findings of the comparison indicate that the distinction between both sets is just in the scenario of a rapid entry velocity due to the motion of both the upper and lower walls with high entry velocity result to alterations in direction of the flow. Regarding the remaining scenarios, there are almost no substantial changes. When both sides channel are immovable, these findings in regular flow, yet in the event of moveable channels' walls findings in eddy forming. Nevertheless, when both the top and bottom walls are shifting in opposite direction of the flow, these findings in turbulent flow, and the

development of a vortex alongside of the shifting wall is bigger than the constant wall, as illustrated in Figs.28 to 31.

However, wavy channel forms with varied inlet velocities suggested the maximum velocity compared with other channel forms from (6, 3, and 0.3 m/s) resulting in an increment of the velocity from 0.333 to 6.18 m/s along with other channel forms recording about equivalent increasing ratio. Moreover, Figs.28 to 31 illustrate the velocity distribution for the parallel form in example 1 with 0.3 m/s input velocity showed notable changes when compared to other velocities.

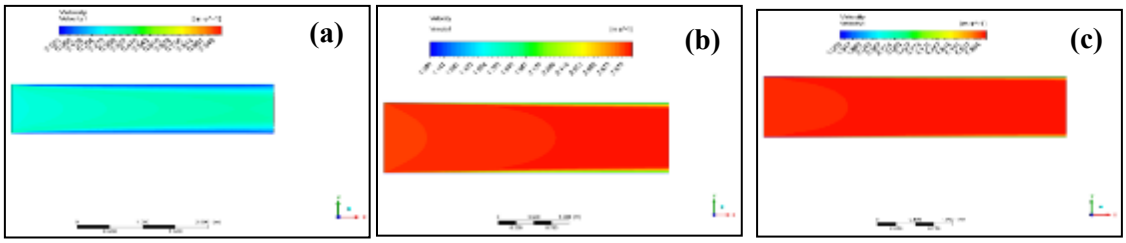


**Fig. 28. Velocity for parallel channels geometry for set 4 cases: (a) 1; (b) 2; (c) 3.**

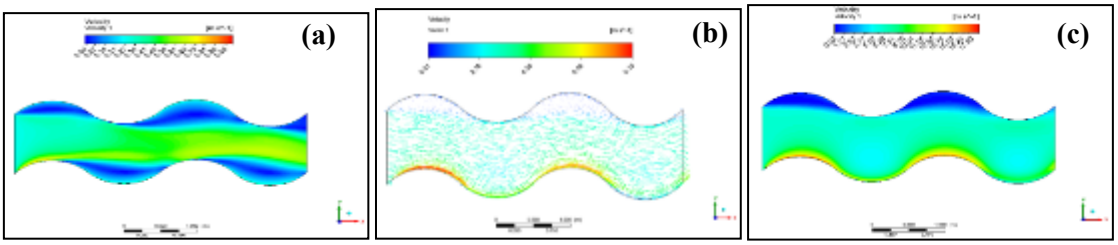


**Fig. 29. Velocity for wavy channels geometry set 4 cases: (a) 1; (b) 2; (c) 3.**

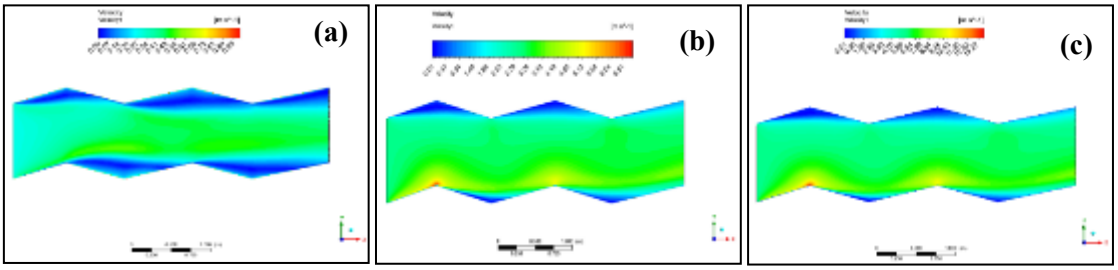


**Fig. 30. Velocity for zigzag channels geometry set 4 cases: (a) 1; (b) 2; (c) 3.**

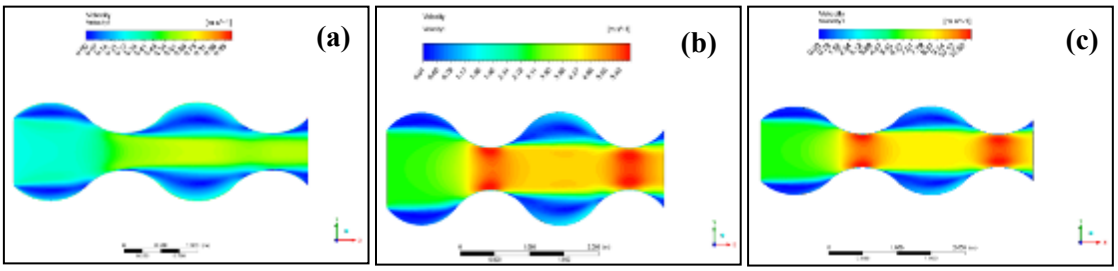


**Fig. 313. Velocity for curvature channels geometry set 4 cases: (a) 1; (b) 2; (c) 3.**

The variations in pressure and input velocity for different channel configurations for set 4 with adjustable walls of channel are shown in Figs.32 to 35. The findings show that curve channels have the maximum-pressure magnitude for all selected entry velocities and that increasing the

inlet velocity also findings in an increase in pressure. The greatest pressure recorded for curve channels was 3384.853 MPa, which is less than the greatest pressure for fixed channels' wall with the same height and entry velocity, which has been 2831.92 MPa.

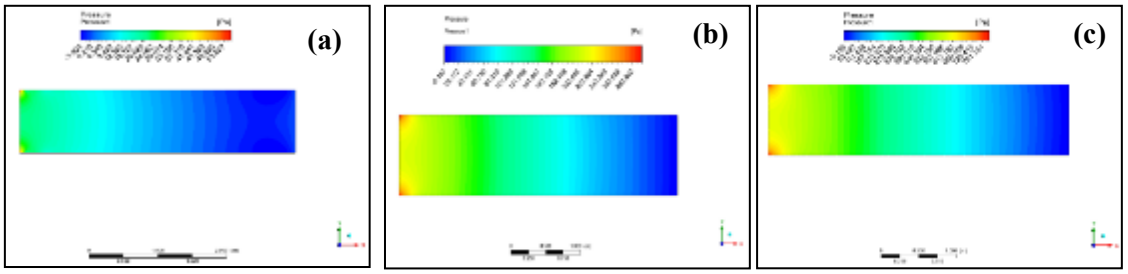


**Fig. 32. Pressure for parallel channels geometry set 4 cases: (a) 1; (b) 2; (c) 3.**

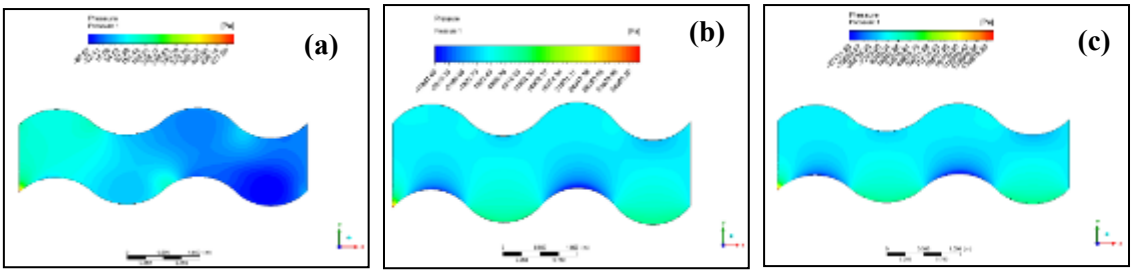


**Fig. 33. Pressure for wavy channels geometry set 4 cases: (a) 1; (b) 2; (c) 3.**

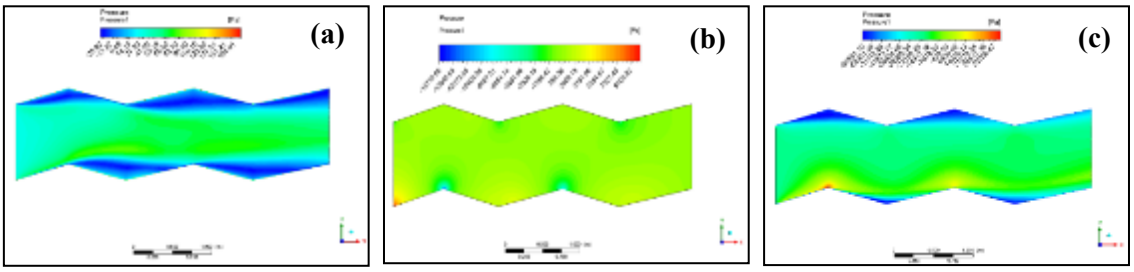


**Fig. 34. Pressure for zigzag channels geometry set 4 cases: (a) 1; (b) 2; (c) 3.**

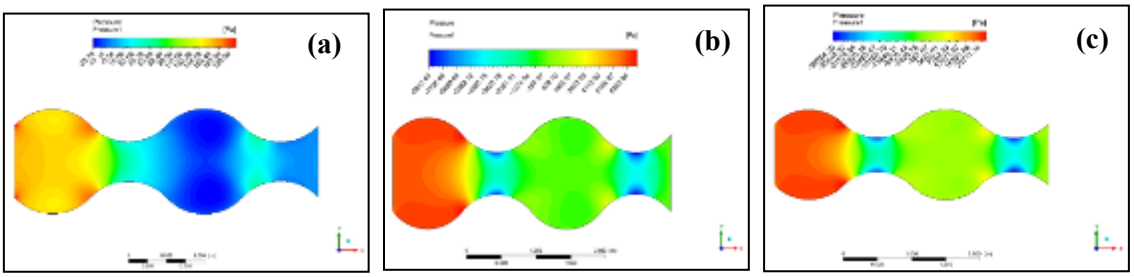


**Fig. 35. Pressure for curvature channels geometry set 4 cases: (a) 1; (b) 2; (c) 3.**

## 4. CONCLUSION

Results indicate that the influence of the channel geometry on flow characteristics in open channels is very important. The optimization of open-channel designs can be directly assisted by numerical simulations, the results from which are as follows:

- The highest outlet velocity of 6.18 m/s was generated by wavy channel, indicating its suitability for application with requirement on maximum flow efficiency. The zigzag channel

on the other hand, had a constant lowest velocity (3.33 m/s at the maximum inlet velocity of 6 m/s) –supporting their applicability to slower flow systems.

- In the case of parallel and zigzag channels, incrementing the height channel (from 0.5 to 1.5 m) significantly increased outlet velocities for inlet velocities of 0.3, 3 and 6 m/s. At 6m/s inlet velocity, for these configurations, outlet velocity became 13.78 m/s for curved geometry. For wavy and curved channels, however, the outlet velocity decreased with the increase in height at 0.3 and 3 m/s inlet velocities with a reduction to 5.16 m/s for the wavy channel at an inlet velocity of 3 m/s (Figures S3(b) and S4).
- In the curved channel, the maximum pressure was obtained at an inlet velocity of 0.3 m/s which was 3384.85 MPa indicating a great potential for high pressure holding applications. In contrast, the pressure drop in all inlet velocities decreased with an increase in parallel and zigzag channels height which is offset against systems where pressure relief is necessary.
- Higher outlet velocities were achieved by increased inlet velocity for all channel cross sections. For example, wavy channel created an outlet velocity of 6.18 m/s for an inlet velocity of 6 m/s as opposed to only 0.333 m/s at an inlet velocity of 0.3 m/s.

In conclusion, the wavy channel, achieving velocities up to 6.18 m/s, is recommended for designs prioritizing high velocity and stable pressure. Meanwhile, the curved channel's ability to maintain high pressure makes it advantageous for pressure-intensive applications. Future work should investigate the energy efficiency and flow stability of these configurations under varying operational conditions.

## 5. REFERENCES

Al-Bedyry, N. K., Kadim, M. A. A., Hussein, S. H., Al-Khafaji, Z. S., & Al-Husseinawi, F. N. (2023). Experimental establishing of moving hydraulic jump in a trapezoidal channel. Civil Engineering Journal, 9(4), 873–881.

Al-Khafaji, Z., Hafedh, A. A., Al-Bedyry, N. K., & Hussien, S. A. (2022). Utilizing of shields factors for sedimentation movements and drainage channels at the middle of Iraq (as a case study). Periodicals of Engineering and Natural Sciences, 10(1), 666–677.

Al-Naely, H., Al-Khafaji, Z., & Khassaf, S. (2019). Effect of opening holes on the hydraulic performance for crump weir. International Journal of Engineering, 31(12), 2022–2027. https://doi.org/10.5829/ije.2018.31.12c.05

Al-Naely, H., Majdi, A., & Al-Khafaji, Z. (2019). A study of the development of the traditional Crump Weir by Adding Opening Holes within the weir body.

Bahaidarah, H. M. S. (2009). Fluid flow and heat transfer characteristics in sharp edge wavy channels with horizontal pitch. Emirates Journal for Engineering Research, 14(1), 53–63.

Benedini, M., & Tsakiris, G. (2013). Water quality modelling for rivers and streams. Springer Science & Business Media.

Harikrishnan, S., & Tiwari, S. (2020). Simulation of fully developed flow and heat transfer in wavy channels using OpenFOAM. In Advances in Mechanical Engineering (pp. 869–877). Springer.

Harikrishnan, S., Kumar, P., & Tiwari, S. (2021). Flow transition in periodically fully developed wavy channels. Physics of Fluids, 33(7), 73605.

Khazaee, I., & Mohammadiun, M. (2012). Effect of flow field on open channel flow properties using numerical investigation and experimental comparison. International Journal of Energy and Environment (Print), 3.

Khlewee, A. S., Alaiwi, Y., Jasim, T. A., Mahdi, M. A. T., Hussain, A. J., & Al-Khafaji, Z. (2024). Numerical investigation of nanofluid-based flow behavior and convective heat transfer using helical screw.

Kumari, B., & Kumar, N. (2022). Principle of Bernoulli's Equation and its Applications. NeuroQuantology, 20(10), 5078.

Memon, A. A., Memon, M. A., Bhatti, K., Alotaibi, H., Hamed, Y. S., Shaikh, G. M., & Khan, I. (2021). Computational Analysis of Fluid Flow through a Sine-Curved Channel with High Reynolds Number. Mathematical Problems in Engineering, 2021.

Nezu, I., & Nakagawa, H. (2017). Turbulence in open-channel flows. Routledge.

Roshankhah, R., Pelton, R., & Ghosh, R. (2023). Optimization of fluid flow in membrane chromatography devices using computational fluid dynamic simulations. Journal of Chromatography A, 1699, 464030.

Seis, C. (2017). A quantitative theory for the continuity equation. Annales de l'Institut Henri Poincaré C, Analyse Non Linéaire, 34(7), 1837–1850.

Stebbins, S. J., Loth, E., Broeren, A. P., & Potapczuk, M. (2019). Review of computational methods for aerodynamic analysis of iced lifting surfaces. Progress in Aerospace Sciences, 111, 100583.

Tao, H., Abba, S. I., Al-Areeq, A. M., Tangang, F., Samantaray, S., Sahoo, A., Siqueira, H. V., Maroufpoor, S., Demir, V., & Bokde, N. D. (2024). Hybridized artificial intelligence models with nature-inspired algorithms for river flow modeling: A comprehensive review, assessment, and possible future research directions. Engineering Applications of Artificial Intelligence, 129, 107559.

Tao, H., Al-Khafaji, Z. S., Qi, C., Zounemat-Kermani, M., Kisi, O., Tiyasha, T., Chau, K.-W., Nourani, V., Melesse, A. M., & Elhakeem, M. (2021). Artificial intelligence models for suspended river sediment prediction: state-of-the art, modeling framework appraisal, and proposed future research directions. Engineering Applications of Computational Fluid Mechanics, 15(1), 1585–1612.

Tokgoz, N. (2019). Experimental and numerical investigation of flow structure in a cylindrical corrugated channel. International Journal of Mechanical Sciences, 157, 787–801.

Tran, N., Chang, Y.-J., Teng, J., & Greif, R. (2017). A study on five different channel shapes using a novel scheme for meshing and a structure of a multi-nozzle microchannel heat sink. International Journal of Heat and Mass Transfer, 105, 429–442.

Wu, B. (2015). The influence of the cross section shape on channel flow : modeling , simulation and experiment Signal Image parole Télécoms ( SIPT ) Annemie Van Hirtum laboratoire Grenoble Image Signal parole Automatique l ' école doctorale Electronique Electrotechnique.

Zakhour, G., Weisenburger, P., & Salvaneschi, G. (2023). Type-checking CRDT convergence. Proceedings of the ACM on Programming Languages, 7(PLDI), 1365–1388.

Zhang, L. Y., Duan, R. J., Che, Y., Lu, Z., Cui, X., Wei, L. C., & Jin, L. W. (2022). A numerical analysis of fluid flow and heat transfer in wavy and curved wavy channels. International Journal of Thermal Sciences, 171, 107248.